



High-performance sulfosuccinic acid cross-linked PVA composite pervaporation membrane for desalination

Rui Zhang, Bin Liang, Ting Qu, Bing Cao & Pei Li

To cite this article: Rui Zhang, Bin Liang, Ting Qu, Bing Cao & Pei Li (2019) High-performance sulfosuccinic acid cross-linked PVA composite pervaporation membrane for desalination, *Environmental Technology*, 40:3, 312-320, DOI: [10.1080/09593330.2017.1388852](https://doi.org/10.1080/09593330.2017.1388852)

To link to this article: <https://doi.org/10.1080/09593330.2017.1388852>



Published online: 25 Oct 2017.



Submit your article to this journal [↗](#)



Article views: 904



View related articles [↗](#)



View Crossmark data [↗](#)



Citing articles: 22 View citing articles [↗](#)



High-performance sulfosuccinic acid cross-linked PVA composite pervaporation membrane for desalination

Rui Zhang*, Bin Liang*, Ting Qu, Bing Cao and Pei Li

College of Materials Science and Engineering, Beijing University of Chemical Technology, Beijing, People's Republic of China

ABSTRACT

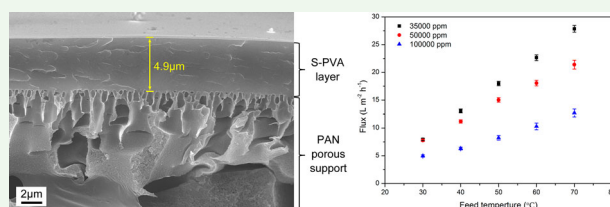
Pervaporation (PV), as a novel technology, has shown great promise in fresh water production from salty water. However, the low water flux of the present membranes hinders their practical applications. Here, a new type of PV composite membrane, consisting of a selective skin layer fabricated from poly(vinyl alcohol) (PVA) cross-linked by sulfosuccinic acid and a porous support layer using a commercial polyacrylonitrile (PAN) ultrafiltration membrane, was developed for applications in desalination. The separation performance of S-PVA/PAN composite PV membranes with different S-PVA layer thicknesses was tested in detail. The best result showed a water flux of $27.9 \text{ kg m}^{-2} \text{ h}^{-1}$ with a salt rejection of 99.8%, which was obtained at a vacuum of 100 Pa and temperature of 70°C when separating a 35,000 ppm NaCl solution. The S-PVA/PAN composite membranes could also be used for the desalination of high-concentration (100,000 ppm) NaCl solutions with a water flux of $11.2 \text{ kg m}^{-2} \text{ h}^{-1}$ with a salt rejection of 99.8%. Moreover, a stable desalination performance was obtained for a 120 h operation time. This study shows the possibility of using PV in desalination applications for seawater, brackish water and reverse osmosis concentrate treatment.

ARTICLE HISTORY

Received 18 July 2017
Accepted 19 September 2017

KEYWORDS

Sulfosuccinic acid; cross-linked PVA; pervaporation desalination; water permeance; water permeability






1. Introduction

Shortage of water resource is one of the world's most concerning problems, which is threatening the lives and development of humans [1,2]. Presently, how to provide sufficient and safe drinking water has become a challenge. Seawater desalination is an important technology for solving the water crisis [3–6]. Since membrane separation technology has many advantages, such as a low energy cost and a high efficiency, it is widely used in desalination applications. Nowadays, reverse osmosis (RO) has become the most applied seawater desalination technology [7–11]. However, RO has limitations to treat high concentrated salt water due to the high trans-membrane pressure required for overcoming the osmotic pressure. It increases the energy cost of the RO process and reduces its economic efficiency. Moreover, the discharge of concentrated seawater as a RO byproduct

may lead to ecology issues. As the energy requirement for the pervaporation (PV) process is independent of the salt concentration in the water, PV membranes have the potential to treat concentrated salt water and reduce the amount of discharged brine water. Thus, PV for desalination has attracted widespread attention [12–15].

PV is a membrane-based separation approach that usually separates different components in a liquid mixture according to their difference in solubility and diffusivity in a dense membrane [16]. In the process of PV, the feed solution is in direct contact with the feed side of the membrane and the permeate is desorbed from the permeate side in a vapor state. Diffusion through the PV membrane is driven by a concentration gradient of the solute between the feed solution and the permeate vapor. The concentration gradient is created by applying

CONTACT Bing Cao  lipei@mail.buct.edu.cn; Pei Li  bcao@mail.buct.edu.cn  College of Materials Science and Engineering, Beijing University of Chemical Technology, Chaoyang District North Third Ring Road 15, Beijing 100029, People's Republic of China

*These authors contributed equally to this work.

a vacuum or sweeping a gas to the membrane permeate side. The solution-diffusion mechanism is widely accepted to describe mass transport in the PV process [17,18]. According to this mechanism, PV occurs in the following steps: (1) the components in the feed are dissolved into the membrane surface, (2) the components diffuse through the PV membrane and (3) the components desorb from the permeate side and diffuse to the vapor phase [19]. PV membranes are widely studied in the dehydration of organic solvents and the removal of volatile organic compounds from aqueous feeds [20–25].

Poly(vinyl alcohol) (PVA) has been extensively studied both in academia and industry for PV applications. Its high hydrophilicity promotes the transport of water molecules and mitigates the membrane fouling by hydrophobic organic compounds. Since PVA is soluble in water, it needs to be cross-linked to increase the stability in water. In most cases, PVA is chemically cross-linked using bifunctional or multifunctional acids, aldehydes or acyl chlorides [26–28]. Previous studies have shown that PV membranes containing sulfonated groups showed enhanced separation performance for ethanol dehydration, because the sulfonic acid groups could increase the hydrophilicity of the polymer [29,30]. However, the water fluxes of these sulfonated PV membranes at high water concentration conditions were not reported. Baker et al. suggested reporting PV data in terms of permeability, permeance and selectivity [31]. In this way, the intrinsic water transport properties of different PV membranes can be compared since permeability and permeance are based on the normalized membrane driving force. If assuming water permeability and permeance are independent to the water concentration in feed, we can conclude that PV membranes having high performances in dehydration applications shall also show high water fluxes when they are applied to separate salt waters which have high water concentrations. In this study, we prepared sulfosuccinic acid (SSA) cross-linked PVA composite membranes using the porous PAN membrane as the substrate. The PV desalination properties of the S-PVA/PAN composite membranes were investigated. The effects of the SSA concentration, the thickness of the S-PVA layer to the desalination properties were studied. And the water permeance and permeability of the S-PVA/PAN composite membranes were calculated and compared with other PV membranes.

2. Experimental section

2.1. Materials

PVA (124,000 Da), with a hydrolysis degree of 99.4%, and NaCl were purchased from Sinopharm Chemical Reagent

Co., Ltd (China). SSA (50% aqueous solution) was purchased from Aldrich (USA). The PAN ultrafiltration membrane was obtained from Ande Membrane Separation Technology & Engineering Co., Ltd. All chemicals were used as received. Deionized (DI) water ($5.1 \mu\text{S cm}^{-1}$ at 20°C) was used to prepare the PVA solution and the aqueous salt solutions.

2.2. Preparation of the S-PVA films and S-PVA/PAN composite membranes

The SSA cross-linked PVA films were prepared using a solution-casting method [32]. Specifically, a powder of PVA (4 g) was first dissolved in DI water (100 mL) at 95°C . The PVA solution (4 wt%) was allowed to cool to room temperature and the pH of the PVA solution was adjusted to a value of 1.7 ± 0.1 by adding HCl (1 M) solution dropwise. Then, a predetermined amount of SSA was added to the PVA solution which was then placed in a Teflon dish. The S-PVA dense film formed after being air-dried for 3 days and then was cross-linked at 80°C for 2 h in a fan-forced oven. The mechanism of the reaction is shown in Figure 1. Using this method, the S-PVA dense films with different SSA concentrations from 6 to 36 wt% were prepared and used for Fourier-transform infrared (FTIR), thermogravimetric analysis (TGA), differential scanning calorimetry (DSC), water contact angle and water uptake measurements. The S-PVA/PAN composite membranes were prepared using a dip-coating method [33]. First, the PAN ultrafiltration membrane is smooth on the surface of the glass plate,

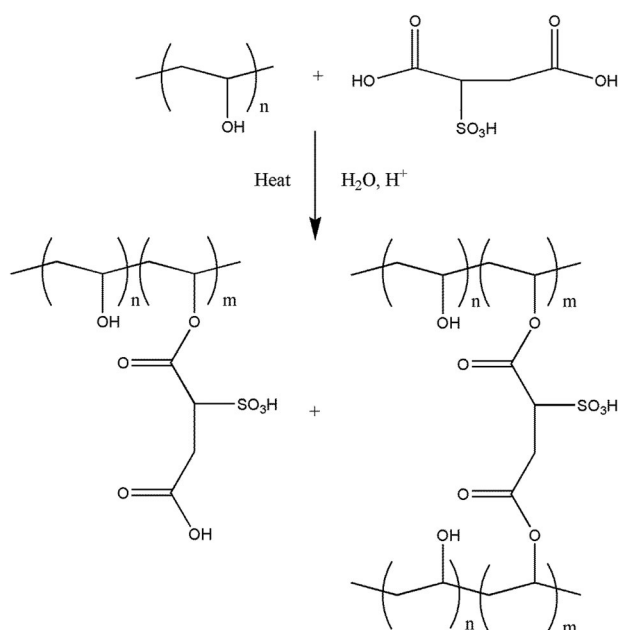


Figure 1. Mechanism of the reaction between PVA and SSA.

and then fit the membrane all around with the waterproof tapes. Dip the membrane horizontally into the PVA solution for 10s, then remove it horizontally and dry naturally. PVA is coated on one side of PAN ultrafiltration membrane. The thickness of the S-PVA coating layers was controlled by adjusting the polymer concentrations of the SSA/PVA coating solutions. After the dip-coating treatment, the S-PVA/PAN composite membranes were heated at 80°C for 2 h in a fan-forced oven to cross-link the S-PVA layers. The thickness of the S-PVA skin layer was measured based on the scanning electron microscopy images using image-processing software (accuracy $\pm 0.2 \mu\text{m}$). An average of five measurements at different locations of each sample was taken as the sample thickness. The S-PVA/PAN composite membranes were used for PV measurements.

2.3. Characterization

Attenuated total reflectance Fourier-transform infrared (ATR-FTIR) spectra of the S-PVA films were recorded on a Perkin-Elmer Spectrum 2000 FTIR instrument (USA) in the range of 4000–650 cm^{-1} with the resolution of 8 cm^{-1} . TGA was conducted by Perkin-Elmer Pyris 1 thermogravimetric analyzer (USA) from 30°C to 800°C at 10°C min^{-1} under nitrogen atmosphere. DSC was probed on Perkin-Elmer Pyris-1 differential scanning calorimeter (USA) to assess the glass transition temperature (T_g) of the PVA and S-PVA samples. The sample was first heated to 40°C at 10°C min^{-1} . After being equilibrated for 10 min, the sample was heated to 200°C at 10°C min^{-1} . The static contact angle of water was obtained at room temperature using a contact angle goniometer (JC2000C Contact Angle Meter, Powereach Co., Shanghai, China). Morphologies of the membranes were observed using field emission scanning electron microscope (FESEM, Hitachi S-4700, Japan) after being freeze-fractured in liquid nitrogen and then sputtered with gold. Energy-dispersive X-ray spectrometry (EDS) was performed using an EDAX detector on a Hitachi S-4700 microscope with a voltage of 15 kV and a working distance of 15 mm.

2.4. Measurements of water uptakes of the S-PVA films

The dried PVA and S-PVA films were immersed in DI water to reach the absorption equilibrium for 48 h at room temperature. The samples were weighed (W_s) after quickly removing the surface water. Then samples were dried in an oven at 60°C for 48 h and then weighed (W_d) again. Three independent tests were conducted on each sample. The water uptake (S) of

membrane was calculated according to Equation (1) [34]:

$$S = \frac{W_s - W_d}{W_s} \times 100\%, \quad (1)$$

2.5. Evaluation of PV performances of the S-PVA/PAN composite membranes

The PV experiments were conducted using a lab-made pervaporation unit with an effective permeation area of 14 cm^2 . The detail information of the equipment can be found in reference [35]. In a typical experiment, an NaCl solution with the predetermined salt concentration of 35,000, 50,000 or 100,000 ppm was pre-heated to the required temperature and then fed into the pervaporation unit. The membrane driving force was imposed by applying vacuum in the permeate side of 100 Pa and the permeate was collected in a liquid-nitrogen cold trap.

The weight of permeate (W) in a unit of kg, membrane effective permeation area (A) in a unit of m^2 and permeate time (t) in a unit of h were used to estimate the membrane water flux (J) in a unit of $\text{kg m}^{-2} \text{h}^{-1}$ using Equation (2):

$$J = \frac{W}{A \times t}. \quad (2)$$

The membrane salt rejection (R) was calculated by using Equation (3):

$$R = 1 - \frac{C_p}{C_f} \times 100\%, \quad (3)$$

where c_f (ppm) and the c_p (ppm) are the NaCl concentrations in the feed and permeate solutions, respectively. Concentration of NaCl in the feed was controlled by dissolving a known amount of NaCl in 1 L DI water. The NaCl concentration in the permeate was estimated using an indirect method, since salt could not vaporized into the vapor phase and be collected in the cold trap. Specifically, after the pervaporation test, the permeate side of the membrane was flushed by a known amount of DI water. Then the salt concentration in washing water was measured using an Oakton® Con 110 conductivity meter. After that, the moles of NaCl could be calculated by knowing the concentration of NaCl and volume of the washing water. Consequently, C_p was calculated by knowing the moles of NaCl in the permeate side of the membrane and the volume of the water collected in the cold trap.

The water permeances of the S-PVA/PAN composite membranes were calculated based on the water vapor flux and the pressure difference between the water vapor pressure of the feed side and the permeate side

using the following equation:

$$\bar{P}_w = \frac{J_v}{\Delta p}, \quad (4)$$

where J_v is the water vapor flux ($\text{cm}^3(\text{stp})/(\text{cm}^2\text{s})$); Δp is the trans-membrane pressure difference of the water vapor (cmHg); \bar{P}_w is the water permeance in a unit of GPU ($1 \text{ GPU} = 1 \times 10^{-6} \text{ cm}^3(\text{stp})/(\text{cm}^2 \text{ s cmHg})$). The water permeability was calculated using the following equation:

$$P_w = \bar{P}_w \times L, \quad (5)$$

where L is the S-PVA layer thickness (cm) and P_w is the water permeability (barrer) ($1 \text{ barrer} = 1 \times 10^{-10} \text{ cm}^3(\text{stp}) \text{ cm}/(\text{cm}^2 \text{ s cmHg})$).

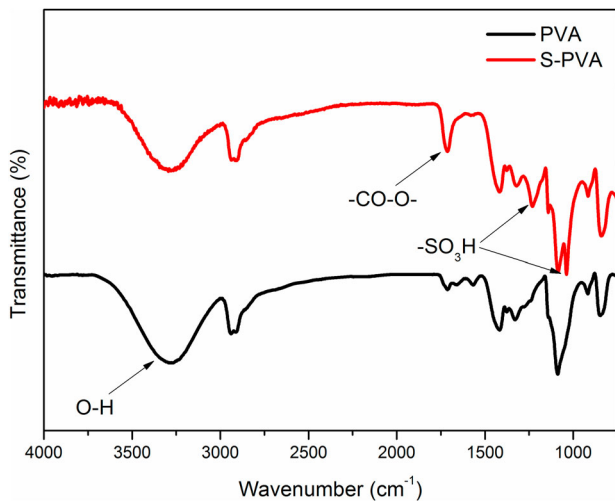


Figure 2. ATR-FTIR spectra of the PVA and S-PVA samples.

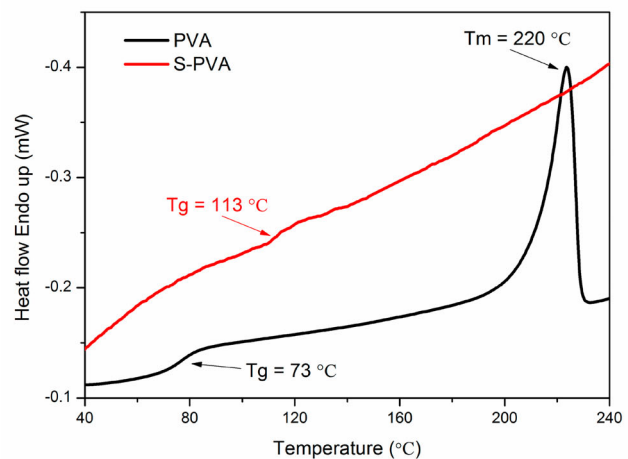
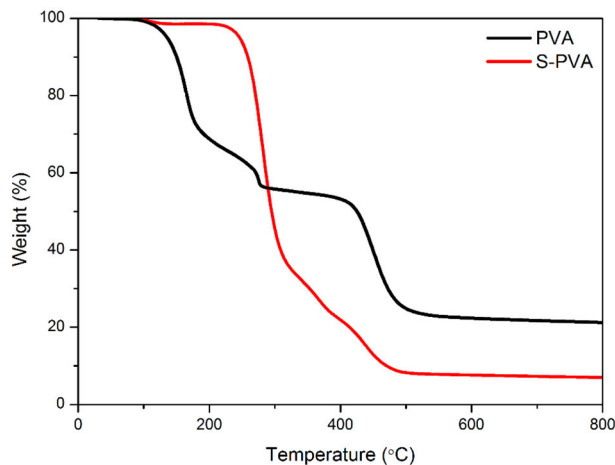


Figure 3. (a) TGA graphs for the PVA and S-PVA samples, (b) DSC curves for the PVA and S-PVA samples.

3. Results and discussion

3.1. ATR-FTIR spectroscopy

The chemical structure of the PVA and 18 wt% SSA cross-linked S-PVA film are investigated by ATR-FTIR spectra as shown in Figure 2. The pristine PVA film shows two broad peaks at 3400 and 2900 cm^{-1} , respectively, representing the hydrogen-bonded hydroxyl group and a broad alkyl C–H stretching band, respectively. The peak at 1100 cm^{-1} is assigned to the C–O stretching vibration of the secondary alcohol (–CH–OH) of PVA. In addition, a small and sharp peak at 1710 cm^{-1} represents the residual vinyl acetate repeating units (–CO–O–) of the PVA polymer. For the cross-linked S-PVA film, the peaks at 1030 and 1226 cm^{-1} represent the S = O (asym) and S = O (sym) bonds of the sulfonic acid group, respectively [36]. The results confirm that the sulfonic acid groups are incorporated and the cross-linking network forms.

3.2. Thermal stability

Figure 3(a) shows that the pristine PVA polymer has two weight loss stages. The first one occurs at a temperature range from 80°C to 140°C which is attributed to the loss of absorbed water. The second weight loss of 80 wt% occurs at temperatures ranging from 200°C to 350°C , which is attributed to the elimination of hydroxyl groups and hydrogen atoms from the PVA molecules. For the 18 wt% SSA cross-linked S-PVA polymer, the first weight loss happens at temperatures from 140°C to 240°C . This weight loss is due to the loss of absorbed water or water molecules generated as by-products from further esterification of the S-PVA polymer. The second broad transition occurs at temperatures between 260°C and 350°C , which is attributed to the de-sulfonation and dissociation of the ester bond (RCOO–R') of S-PVA

[37]. Finally, the third weight loss occurs at temperatures between 400°C and 600°C, which is attributed to the thermal decomposition of polymer chains. Based on the TGA result, the cross-linked S-PVA polymer has higher thermal stability than the pristine PVA polymer.

Figure 3(b) shows the DSC curves for the pristine PVA and 18 wt% SSA cross-linked S-PVA films. The pristine PVA polymer has both glass transition temperature (T_g) and melting temperature (T_m) at 73°C and 220°C, respectively. The cross-linked S-PVA polymer has a higher T_g of 113°C, but does not show the melting peak. This result indicates that the cross-link reaction prohibits the formation of the crystalline structure of the PVA polymer and increases the polymer chain rigidity [38].

3.3. Water uptake and contact angle

The pristine PVA polymer is soluble in hot water. Therefore, it will be highly swollen by water and cause the leakage of the PVA membrane. After the cross-link treatment, the resulting S-PVA polymer shall have improved stability in water. To compare the stabilities of the cross-linked S-PVA and pristine PVA polymer in water, the water uptakes of the two polymers are measured. Table 1 shows that the water uptake of the pristine PVA is very high (194.3%). But for the 18 wt% SSA cross-linked S-PVA polymer, the water uptake decreases to 83.5%. This indicates that the cross-linked PVA polymer network reduces the swelling of the PVA polymer by water molecules.

Generally, pure PVA and S-PVA are hydrophilic. The pure PVA film is very hydrophilic, with a water contact angle of 44.3° as shown in Table 1. After being cross-linked by SSA, the contact angle increases to 77.1°, indicating that the surface of the S-PVA sample has become more hydrophobic. When SSA is incorporated with PVA, the cross-linking between the PVA and the SSA led to the consumption of -OH groups; therefore, the hydrophilicity decreases [39].

3.4. Morphology of the S-PVA/PAN composite membranes

As shown in Figure 4(a), a smooth and defect-free S-PVA skin layer is formed on top of the PAN ultrafiltration support. Moreover, the EDS spectrum confirms the

Table 1. The water uptake and contact angle of the PVA and 18 wt% SSA cross-link S-PVA films.

Sample ID	Water uptake (%)	Water contact angle (°)
PVA	194.3 ± 10.7	44.3 ± 2.7
S-PVA	83.5 ± 5.1	77.1 ± 3.0

introduction of sulfonic acid groups in the S-PVA layer. Figure 4(b) shows the S-PVA/PAN composite membrane has a dense S-PVA layer of 4.9 μm with a porous PAN substrate. There is intact adhesion between the S-PVA skin layer and the PAN ultrafiltration support layer.

3.5. Effect of the concentration of SSA in S-PVA layer on the separation performance

Figure 5 shows that the water flux first increases as the concentration of SSA increases from 6 to 18 wt% and then decreases as the SSA concentration further increases to 36 wt%. The salt rejections of all membranes are higher than 99.8%. The increase in the SSA concentrations corresponds to the increase in the sulfonic acid concentration. And a high SSA concentration in PVA results in a high cross-linking density of S-PVA. It leads to a low diffusivity of the water molecules in the S-PVA layer. However, a high content of sulfonic acid group favors the facilitating of transport of water molecules in the S-PVA layer. The experiment result shows that at low SSA concentrations (below 18 wt%), the promotion to the water transport by the incorporation of the sulfonic acid groups overplays the restriction to water diffusion by cross-linking. However, at a high SSA concentration (36 wt%), the highly cross-linked S-PVA polymer network restricts the water diffusion and

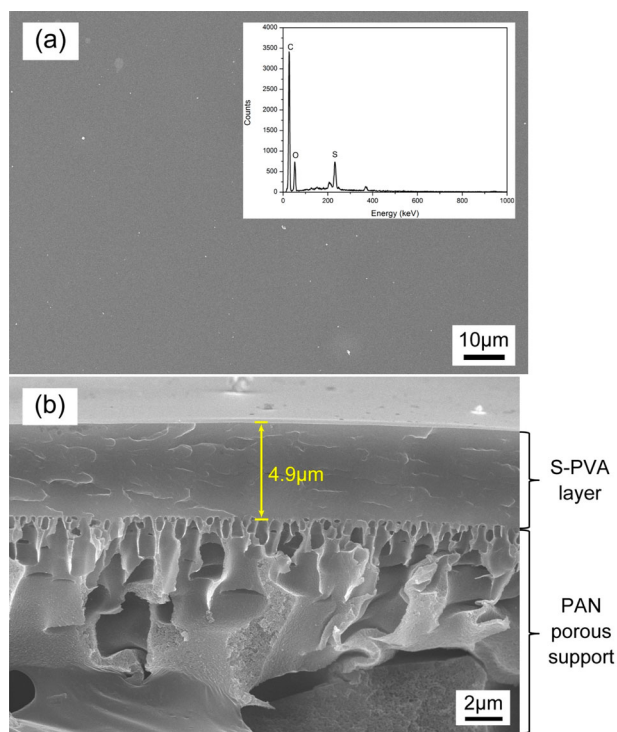


Figure 4. (a) Surface SEM image and EDS spectra of the S-PVA/PAN composite membrane; (b) cross-sectional SEM image of the S-PVA membrane.

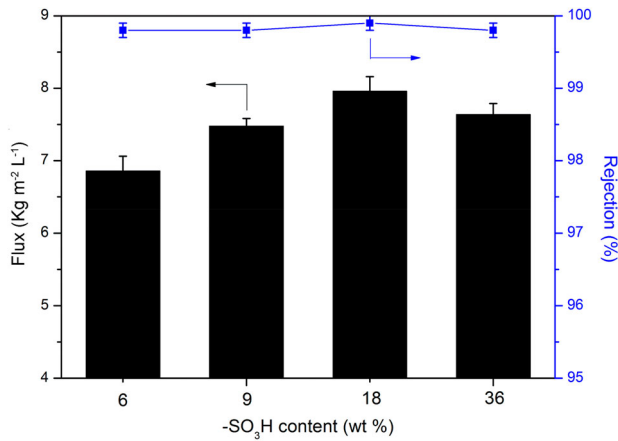


Figure 5. PV testing results using the S-PVA membrane cross-linked by different amounts of SSA (S-PVA skin layer thickness: 4.9 μm , NaCl feed solution concentration: 35,000 ppm, feed temperature: 30°C, vacuum: 100 Pa).

results in a decreased water flux. In terms of salt rejection, the entire cross-linked PVA network structure exhibits good interception against hydrated ions. Therefore, the 18 wt% SSA cross-linked PVA/PAN composite membrane has the best desalination performance.

3.6. Effect of the skin layer thickness on the separation performance

The 18 wt% S-PVA/PAN composite membrane shows the best desalination property. A series of S-PVA/PAN PV composite membranes with different S-PVA skin layer thicknesses (4.9, 10.5 and 18.4 μm) are prepared to study the relation between the water flux and the S-PVA layer thickness. Figure 6 shows that as the S-PVA layer thickness increases from 4.9 to 18.4 μm , the salt

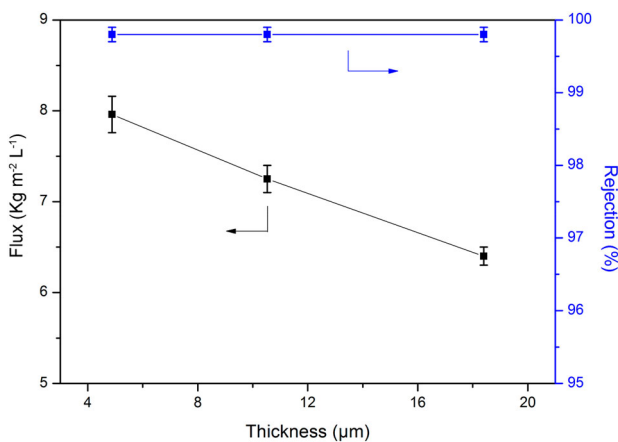


Figure 6. Effect of S-PVA skin layer thickness on the water flux (membrane containing 18 wt% SSA with respect to PVA; NaCl feed solution concentration: 35,000 ppm, feed temperature: 30°C, vacuum: 100 Pa).

rejection is similar (about 99.8%) but the water flux gradually decreases from 7.9 to 6.4 $\text{kg m}^{-2} \text{h}^{-1}$. The mass-transfer mechanism of the PV membrane follows the solution-diffusion model. Then, as the S-PVA layer thickness increases, the mass-transfer resistance also increases [40]. This indicates that a PV membrane with a higher water flux can be obtained by decreasing the thickness of the skin layer while maintaining its structural integrity.

3.7. Effect of feed concentration on separation performance

The feed concentration is believed to directly affect the sorption of its components at the interface between the feed and the membrane surface [41,42]. That is, when the concentration of the component in the feed increases, its concentration in the membrane also increases. Based on the solution-diffusion model, the permeability of water shall increase with the water concentration in the feed. Moreover, the driving force of a PV process is the vapor pressure difference between the feed and permeate side of the membrane. As the salt concentration increases, the saturate water pressure in the feed side shall decrease leading to a decrease in the water flux.

Figure 7 shows that as the salt concentration increases from 35,000 to 100,000 ppm, the water flux decreases from 7.9 to 4.5 $\text{kg m}^{-2} \text{h}^{-1}$. Since the water concentration in the feed decreases from 96.5 wt% to 90 wt%, the corresponding water vapor pressure in the feed decreases from 4.1 to 3.82 kPa. It indicates that the saturate water vapor pressure in the feed side is barely changed. According to the solution-diffusion mechanism, the water flux shall be very similar in all three salt

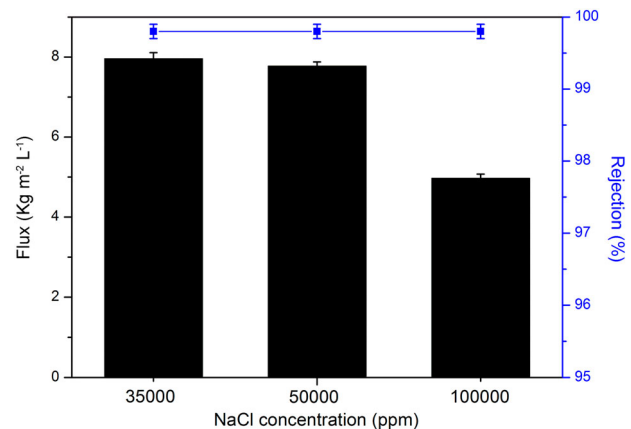


Figure 7. Effect of the feed concentration on the water flux (S-PVA skin layer thickness: 4.9 μm , feed temperature: 30°C, vacuum: 100 Pa).

concentrations. Therefore, we believe that the significant drop in water flux is due to the effect of concentration polarization.

3.8. Effect of feed temperature on water flux

Figure 8(a) shows that there is an exponential increase in water flux with the feed temperature for all three salt concentrations. A high water flux of $27.9 \text{ kg m}^{-2} \text{ h}^{-1}$ is achieved at a feed temperature of 70°C when separating the 35,000 ppm salt solution. This is because the driving force for the PV process is the partial vapor pressure difference between the feed and the permeate. As the feed temperature increases, the water vapor pressure on the feed side increases exponentially [43]. When the vapor pressure on the feed side increases but the vapor pressure on the permeate side is maintained at 100 Pa, the driving force increases; therefore, the water flux increases. In addition, when the feed temperature increases, the mobility of the polymer chains also increases; therefore, the free volume of the membranes increases. According to free volume theory [44], momentary free volumes are created by the thermal motion of polymer chains in an amorphous region. As the temperature increases, the frequency and amplitude of chain motion increase. The polymer-free volumes become larger and water molecules can diffuse through them more easily, thus the water flux increases.

The temperature dependence of the permeate flux for PV generally follows an Arrhenius type relationship [45]:

$$J_i = A_i \exp\left(-\frac{E_{p,i}}{RT}\right), \quad (6)$$

where J_i is the permeate flux of membrane, A_i is the pre-exponential factor, R is the gas constant, T is the absolute

temperature and $E_{p,i}$ is the apparent activation energy for permeation, which depends on both the activation energy for diffusion and the heat of sorption. Figure 8(b) shows the Arrhenius plot of the water flux and feed temperature at different feed concentrations. The results show that the water flux and the reciprocal of the absolute temperature of the feed follow a linear relationship.

3.9. The long-term desalination performance

Figure 9 shows the 120-h continuous desalination performance of the S-PVA/PAN composite membrane. The S-PVA layer thickness of composite membrane used in this test is $4.9 \mu\text{m}$ since it has the best desalination properties among all composite membranes. Both the water flux and the salt rejection are stable in the entire

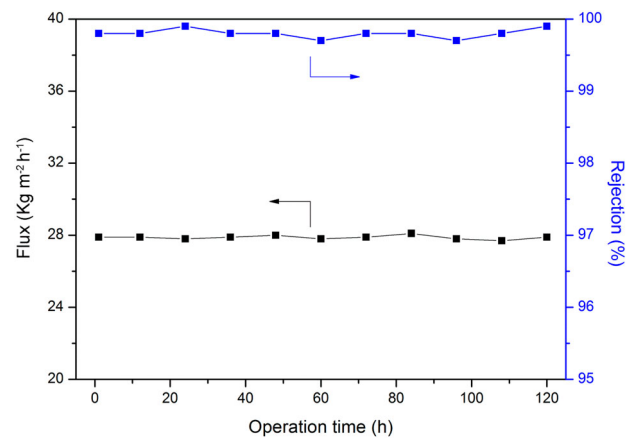


Figure 9. The long-term desalination performance of the S-PVA/PAN composite membrane (the thickness of S-PVA layer is $4.9 \mu\text{m}$, operation temperature: 70°C , feed solution: 35,000 ppm NaCl).

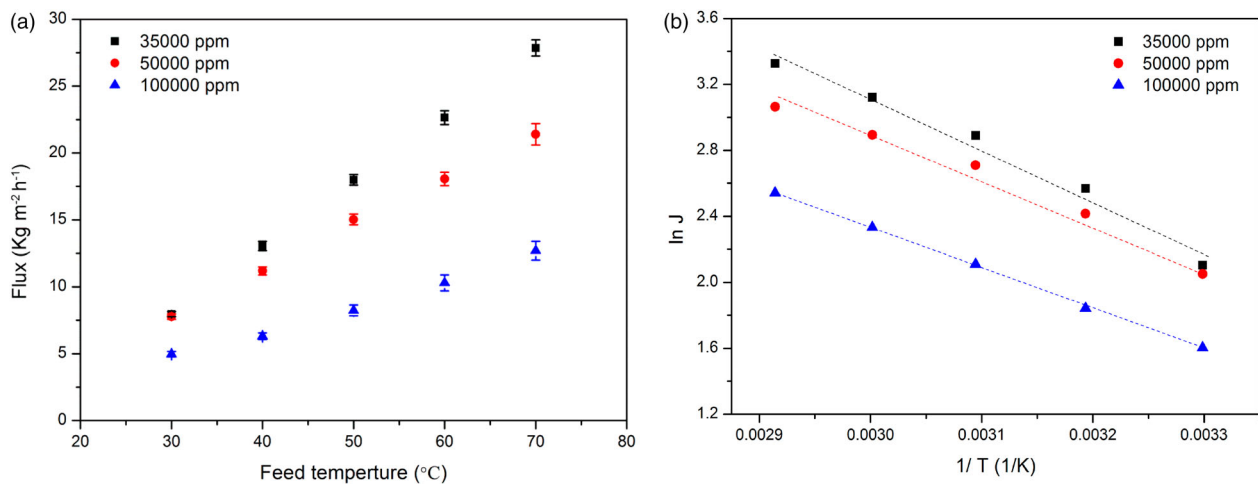


Figure 8. (a) Effect of the feed temperature on the water flux; (b) Arrhenius plot of the water flux at various feed temperatures (S-PVA layer thickness: $4.9 \mu\text{m}$, vacuum: 100 Pa).

Table 2. Comparison of saline–water transport properties of the PV membranes prepared by different groups.

Membrane	Feed solution	Feed temperature (°C)	Dense layer thickness (μm)	Flux (kg m ⁻² h ⁻¹)	Permeance (1 × 10 ⁴ GPU)	Permeability (1 × 10 ⁴ barrer)	Reference
Polyether amide	35,000 ppm NaCl	70	40	1.0	0.16	6.49	44
NaA zeolite membrane	35,000 ppm NaCl	69	–	1.9	0.29	–	13
PVA/Maleic acid/Silica	2000 ppm NaCl	22	6	6.93	17.3	104	14
S-PVA/PAN	35,000 ppm NaCl	70	4.9	27.9	4.3	21.0	This study

experiment period. The result further confirms that the S-PVA skin layer of the composite membrane is stable.

3.10. The comparison of the brine transport properties of the S-PVA/PAN composite membrane with other reported data

The saline–water transport properties of different PV membranes are listed in Table 2. Our S-PVA/PAN composite membrane has the highest water flux among all PV membranes. Moreover, the water permeance and permeability, which are estimated based on the normalized membrane driving force, of the S-PVA/PAN membrane are higher than the Polyether amide and NaA zeolite membrane [14,46]. It may be because the sulfonic acid improves on water transport properties in our membrane. However, the water permeance and permeability of the membranes containing nano-particles (PVA/Maleic acid/Silica [13]) are higher than our membrane. The reason why their water fluxes are lower is because the water concentrations and temperature of their feeds are lower and the dense layer thicknesses of their membranes are higher than our membrane. This tells us the desalination performance can be further improved by adding nano-particles in the selective layer of the PV membrane. This attempt will be made in our future work.

4. Conclusions

In summary, the SSA cross-linked S-PVA/PAN PV composite membranes have been prepared. The sulfonic acid functional groups were successfully introduced into the PVA polymer matrix and the thermal stability of the PVA polymer was enhanced. The water uptake measurements revealed that the swelling degree of the S-PVA polymer in water was greatly suppressed. The water contact angle measurements indicated a slightly reduced but still hydrophilic nature of the cross-linked S-PVA polymer. A water flux of 27.9 kg m⁻² h⁻¹ with a salt rejection of 99.8%, for an NaCl solution with a concentration of 35,000 ppm, was achieved at a 100 Pa vacuum and a feed temperature of 70°C. The membrane also showed good desalination property when using water with high NaCl concentration (100,000 ppm) as feed. These results demonstrated that there was a potential application of

this PV membrane in seawater desalination, brackish water desalination and RO concentrate treatment.

Disclosure statement

No potential conflict of interest was reported by the authors.

Funding

The project was supported by the Higher Education and High-quality and World-class Universities [grant number PY201618] and National Natural Science Foundation of China [grant numbers 51373014, 51403012].

References

- [1] Mccinnis RL, Elimelech M. Global challenges in energy and water supply: the promise of engineered osmosis. *Environ Sci Technol.* 2008;42(23):8625–8629.
- [2] Elimelech M, Phillip WA. The future of seawater desalination: energy, technology, and the environment. *Science.* 2011;333(6043):712–717.
- [3] Zhou M, Nemade PR, Lu X, et al. New type of membrane material for water desalination based on a cross-linked bicontinuous cubic lyotropic liquid crystal assembly. *J Am Chem Soc.* 2007;129(31):9574–9575.
- [4] Zhu H, Wang H, Wang F, et al. Preparation and properties of PTFE hollow fiber membranes for desalination through vacuum membrane distillation. *J Memb Sci.* 2013;446(1):145–153.
- [5] Corry B. Designing carbon nanotube membranes for efficient water desalination. *J Phys Chem B.* 2008;112(5):1427–1434.
- [6] Cohentanugi D, Grossman JC. Water desalination across nanoporous graphene. *Nano Lett.* 2012;12(7):3602–3608.
- [7] Zhang J-W, Fang H, Wang J-W, et al. Preparation and characterization of silicon nitride hollow fiber membranes for seawater desalination. *J Memb Sci.* 2014;450(2):197–206.
- [8] Lee KP, Arnot TC, Mattia D. A review of reverse osmosis membrane materials for desalination – development to date and future potential. *J Memb Sci.* 2011;370(1–2):1–22.
- [9] Chong TH, Wong FS, Fane AG. Enhanced concentration polarization by unstirred fouling layers in reverse osmosis: detection by sodium chloride tracer response technique. *J Memb Sci.* 2007;287(2):198–210.
- [10] Greenlee LF, Lawler DF, Freeman BD, et al. Reverse osmosis desalination: water sources, technology, and today's challenges. *Water Res.* 2009;43(9):2317–2348.
- [11] Bo Z, Zhou H, Milne N, et al. Desalination of seawater ion complexes by MFI-type zeolite membranes: temperature and long term stability. *J Memb Sci.* 2014;453(3):126–135.

- [12] Drobek M, Yacou C, Motuzas J, et al. Long term pervaporation desalination of tubular MFI zeolite membranes. *J Memb Sci.* 2012;415-416(10):816-823.
- [13] Xie Z, Hoang M, Duong T, et al. Sol-gel derived poly(vinyl alcohol)/maleic acid/silica hybrid membrane for desalination by pervaporation. *J Memb Sci.* 2011;383(1-2):96-103.
- [14] Cho CH, Oh KY, Si KK, et al. Pervaporative seawater desalination using NaA zeolite membrane: mechanisms of high water flux and high salt rejection. *J Memb Sci.* 2011;371(1-2):226-238.
- [15] Kuznetsov YP, Kruchinina EV, Baklagina YG, et al. Deep desalination of water by evaporation through polymeric membranes. *Russ J Appl Chem.* 2007;80(5):790-798.
- [16] Jiang LY, Wang Y, Chung T-S, et al. Polyimides membranes for pervaporation and biofuels separation. *Prog Polym Sci.* 2009;34(11):1135-1160.
- [17] Shao P, Huang RYM. Polymeric membrane pervaporation. *J Memb Sci.* 2007;287(2):162-179.
- [18] Berlo AD-V, Vankelecom IFJ, Bruggen BVD. Parameters determining transport mechanisms through unfilled and silicalite filled PDMS-based membranes and dense PI membranes in solvent resistant nanofiltration: comparison with pervaporation. *J Memb Sci.* 2011;374(1-2):138-149.
- [19] Cao B, Henson MA. Modeling of spiral wound pervaporation modules with application to the separation of styrene/ethylbenzene mixtures. *J Memb Sci.* 2002;197(1):117-146.
- [20] Hua D, Rai RK, Zhang Y, et al. Aldehyde functionalized graphene oxide frameworks as robust membrane materials for pervaporative alcohol dehydration. *Chem Eng Sci.* 2017;161:341-349.
- [21] Hua D, Chung T-S. Universal surface modification by aldehydes on polymeric membranes for isopropanol dehydration via pervaporation. *J Memb Sci.* 2015;492:197-208.
- [22] Shi GM, Zuo J, Tang SH, et al. Layer-by-layer (LbL) polyelectrolyte membrane with Nexar™ polymer as a polyanion for pervaporation dehydration of ethanol. *Sep Purif Technol.* 2015;140:13-22.
- [23] Shi GM, Chung TS. Thin film composite membranes on ceramic for pervaporation dehydration of isopropanol. *J Memb Sci.* 2013;448(24):34-43.
- [24] Li J, Ji S, Zhang G, et al. Surface-modification of poly(dimethylsiloxane) membrane with self-assembled monolayers for alcohol permselective pervaporation. *Langmuir.* 2013;29(25):8093-8102.
- [25] Cheng XQ, Konstas K, Doherty CM, et al. Organic microporous nanofillers with unique alcohol affinity for superior ethanol recovery toward sustainable biofuels. *ChemSuschem.* 2017;10(9):1887-1891.
- [26] Guo R, Fang X, Wu H, et al. Preparation and pervaporation performance of surface crosslinked PVA/PES composite membrane. *J Memb Sci.* 2008;322(1):32-38.
- [27] Wu Y, Wu C, Li Y, et al. PVA-silica anion-exchange hybrid membranes prepared through a copolymer crosslinking agent. *J Memb Sci.* 2010;350(1-2):322-332.
- [28] Wu Y, Luo J, Zhao L, et al. QPPO/PVA anion exchange hybrid membranes from double crosslinking agents for acid recovery. *J Memb Sci.* 2013;428(2):95-103.
- [29] Wang X-S, An Q-F, Liu T, et al. Novel polyelectrolyte complex membranes containing free sulfate groups with improved pervaporation dehydration of ethanol. *J Memb Sci.* 2014;452(452):73-81.
- [30] Yuan H-K, Xu Z-L, Shi J-H, et al. Perfluorosulfonic acid-Tetraethoxysilane/polyacrylonitrile (PFSA-TEOS/PAN) hollow fiber composite membranes prepared for pervaporation dehydration of ethyl acetate-water solutions. *J Appl Polym Sci.* 2008;109(6):4025-4035.
- [31] Baker RW, Wijmans JG, Yu H. Permeability, permeance and selectivity: A preferred way of reporting pervaporation performance data. *J Memb Sci.* 2010;348(1-2):346-352.
- [32] Zhang C, Li P, Cao B. Decarboxylation crosslinking of polyimides with high CO₂/CH₄ separation performance and plasticization resistance. *J Memb Sci.* 2017;528:206-216.
- [33] Zhang C, Li P, Cao B. Fabrication of superhydrophobic-superoleophilic fabrics by etching and dip-coating two-step method for oil-water separation. *Ind Eng Chem Res.* 2016;55(17):5030-5035.
- [34] Liang B, Pan K, Li L, et al. High performance hydrophilic pervaporation composite membranes for water desalination. *Desalination.* 2014;347(17):199-206.
- [35] Liang B, Zhan W, Qi G, et al. High performance graphene oxide/polyacrylonitrile composite pervaporation membranes for desalination applications. *J Mater Chem A.* 2015;3(9):5140-5147.
- [36] Kim DS, Park HB, Ji WR, et al. Preparation and characterization of crosslinked PVA/SiO₂ hybrid membranes containing sulfonic acid groups for direct methanol fuel cell applications. *J Memb Sci.* 2004;240(1-2):37-48.
- [37] Chanthad C, Wootthikanokkhan J. Effects of crosslinking time and amount of sulfophthalic acid on properties of the sulfonated poly(vinyl alcohol) membrane. *J Appl Polym Sci.* 2006;101(3):1931-1936.
- [38] Bolto B, Tran T, Hoang M, et al. Crosslinked poly(vinyl alcohol) membranes. *Prog Polym Sci.* 2009;34(9):969-981.
- [39] Tang Z, Wei J, Yung L, et al. UV-cured poly(vinyl alcohol) ultrafiltration nanofibrous membrane based on electrospun nanofiber scaffolds. *J Memb Sci.* 2009;328(1):1-5.
- [40] Hyder MN, Huang RYM, Chen P. Effect of selective layer thickness on pervaporation of composite poly(vinyl alcohol)-poly(sulfone) membranes. *J Memb Sci.* 2008;318(1-2):387-396.
- [41] Jiratananon R, Chanachai A, Huang RYM, et al. Pervaporation dehydration of ethanol-water mixtures with chitosan/hydroxyethylcellulose (CS/HEC) composite membranes : I. Effect of operating conditions. *J Memb Sci.* 2002;195(2):143-151.
- [42] Geng Y, Zhang P, Wang Q, et al. Novel PAN/PVP Janus ultrafine fiber membrane and its application for biphasic drug release. *J Mater Chem B.* 2017;5:5390-5396.
- [43] Peters TA, Poeth CHS, Benes NE, et al. Ceramic-supported thin PVA pervaporation membranes combining high flux and high selectivity; contradicting the flux-selectivity paradigm. *J Memb Sci.* 2006;276(1):42-50.
- [44] Xie Z, Ng D, Hoang M, et al. Separation of aqueous salt solution by pervaporation through hybrid organic-inorganic membrane: effect of operating conditions. *Desalination.* 2011;273(1):220-225.
- [45] Peng F, Lu L, Sun H, et al. Analysis of annealing effect on pervaporation properties of PVA-GPTMS hybrid membranes through PALS. *J Memb Sci.* 2006;281(1):600-608.
- [46] Zwijnenberg HJ, Koops GH, Wessling M. Solar driven membrane pervaporation for desalination processes. *J Memb Sci.* 2005;250(1-2):235-246.